

## ARTICLE

# PERFORMANCE ANALYSIS OF AUTOMATIC CLASSIFICATION OF RETINAL VESSELS INTO ARTERIES AND VEINS

M Anto Bennet<sup>1\*</sup>, S Sankaranarayanan<sup>2</sup>, G Sankarbabu<sup>3</sup>, A Abinayaa<sup>4</sup>, U Mageshwari<sup>5\*</sup>

<sup>1</sup>Professor, <sup>2,3</sup>Asst. Professor, <sup>4,5</sup>UG Students, Department of ECE, VEL TECH, Avadi, Chennai 600 062, Tamil Nadu, INDIA

## ABSTRACT

Our vision reduced in eye due to the presence of Retinal diseases like Exudates (diabetic Retinopathy), Micro aneurysms, and Blood vessel damage. This project mainly concentrates on the symptoms of heart, lung, liver and kidney problems identification using Retinal fundus images. Our proposed work shows that how optic disk elimination and follower the symptom detection. Optic disk is one of the parts which consist of intersection of blood vessels and it also has same characteristics of exudates like yellow color, intensity and contrast. Distinguish the exudates and optic disk is critical one. So only first eliminate the optic disk and follower that exudates detection. This detection method very favorably with existing and promise deployment of these systems. Micro aneurysms are the initial stage of exudates.

## INTRODUCTION

Infection Blood flow in the microvasculature plays a pivotal role in determining the outcome of injury and repair in inflamed tissue. Real-time observation of the kidney microvasculature, including the glomerular capillary tufts, is extremely difficult because of the methodological limitations of currently available microscope optics. In the present study, we attempted to analyze hemodynamic events that occurred in vivo during microvascular regeneration following destruction of the glomerular capillary tuft, functionally and quantitatively by the use of a real-time confocal laser-scanning microscope (CLSM) system [1]. Blood flow in the microvasculature plays a pivotal role in determining the fate of injury and repair of inflamed tissue. Direct observation of the hemodynamic events occurring in the microcirculation under physiological conditions would allow us to deepen our understanding of the precise mechanisms by which inflammation occurs in the microvasculature. Real-time observation of the kidney microvasculature, including the glomerular capillary tuft, however, is extremely difficult because of the methodological limitations of currently available microscope optics. One strategy to observe the glomerular microvasculature in the rat has been performed using hydronephrotic kidneys. Although pathological changes in the blood vessels caused by this better procedure are relatively minor, especially in rats, hydronephrosis is accompanied by a marked decrease in kidney blood flow. To avoid nonphysiological effects of operative procedures, we introduce an intravital real time confocal laser-scanning microscope (CLSM) system, in combination with fluorescent tracer labeling. We report novel findings during hemodynamic changes in the anti-Thy-1 antibody-induced glomerular aneurysms by surveying with this new equipment. Anti-Thy-1.1 nephritis is a good model for analyzing the hemodynamic changes of glomeruli during the course from destruction of microvasculature to resolution of glomerular architecture [2]. The application of CLSM enables the restitution of glomerular and periglomerular hemodynamics, following mesangial damage to be examined. The human lungs are the organs of respiration in humans. Humans have two lungs, a right lung and a left lung. The right lung consists of three lobes while the left lung is slightly smaller consisting of only two lobes (the left lung has a "cardiac notch" allowing space for the heart within the chest). Together, the lungs contain approximately 2,400 kilometers (1,500 mi) of airways and 300 to 500 million alveoli, having a total surface area of about 70 square meters (750 sq ft) to 100 square metres (1076.39 sq ft) (8,4 x 8,4 m) in adults roughly the same area as one side of a tennis court. Furthermore, if all of the capillaries that surround the alveoli were unwound and laid end to end, they would extend for about 992 kilometres (616 mi). The lungs together weigh approximately 2.3 kilograms, with the right lung weighing more than the left. The pleural cavity is the potential space between the two serous membranes, (pleurae) of the lungs; the parietal pleura, lining the inner wall of the thoracic cage, and the visceral pleura, lining the organs themselves—the lungs. The respiratory system includes the conducting zone, which consists of all parts of the airway that conducts air into the lungs. The parenchyma of the lung, only relates to the functional alveolar tissue, but the term is often used to refer to all lung tissue, including the respiratory bronchioles, alveolar ducts, terminal bronchioles, and all connecting tissues [3]. The trachea divides at a junction the carina of trachea, to give a right bronchus and a left bronchus, and this is usually at the level of the fifth thoracic vertebra. The conducting zone contains the trachea, the bronchi, the bronchioles, and the terminal bronchioles. The respiratory system contains the respiratory bronchioles, the alveolar ducts, and the alveoli. The conducting zone and the respiratory components, except the alveoli, are made up of airways with gas exchange only taking place in the alveoli of the respiratory system. The conducting zone is reinforced with cartilage in order to hold open the airways. Air is warmed to 37 °C (99 °F), humidified and cleansed by the conduction zone; particles from the air being removed by the cilia which are located on the walls of all the passageways[4]. The lungs are surrounded and protected by the rib cage shown in [Fig.1].

### KEY WORDS

Confocal Laser Scanning Microscope (CLSM), Fuzzy Inference System (FIS), Adaptive Neuro-fuzzy inference system

Received: 24 October 2016  
Accepted: 20 December 2016  
Published: 15 February 2017

\*Corresponding Author  
Email:  
bennetmab@gmail.com

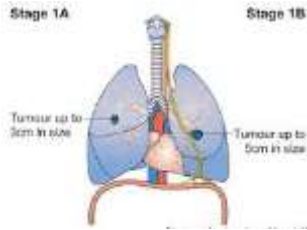


Fig.1: Diagram of Lung

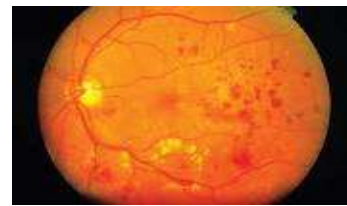


Fig.2: Retina with micro aneurysm formation

MATERIALS AND METHODS

MICROANEURYSM is a tiny area of blood protruding from an artery or vein in the back of eye. These protrusions may open and leak blood into the retinal tissue surrounding it. The problems in Liver are detected through Exudates formation in retina. The liver is a vital organ present in vertebrates and some other animals. It has a wide range of functions, including detoxification, protein synthesis, and production of biochemicals necessary for digestion. The liver is necessary for survival; there is currently no way to compensate for the absence of liver function in the long term, although new liver dialysis techniques can be used in the short term [5]. This gland plays a major role in metabolism and has a number of functions in the body, including glycogen storage, decomposition of red blood cells, plasma protein synthesis, hormone production, and detoxification. It lies below the diaphragm in the abdominal-pelvic region of the abdomen. It produces bile, an alkaline compound which aids in digestion via the emulsification of lipids. The liver's highly specialized tissues regulate a wide variety of high-volume biochemical reactions, including the synthesis and breakdown of small and complex molecules, many of which are necessary for normal vital functions shown in [Fig. 2].

Blood flow left lobe liver tumor

The liver supports almost every organ in the body and is vital for survival. Because of its strategic location and multidimensional functions, the liver is also prone to many diseases [6]. The most common include: Infections such as hepatitis A, B, C, D, E, alcohol damage, fatty liver, cirrhosis, cancer, drug damage (particularly by acetaminophen (paracetamol) and cancer drugs). Many diseases of the liver are accompanied by jaundice caused by increased levels of bilirubin in the system [7]. The bilirubin results from the breakup of the hemoglobin of dead red blood cells; normally, the liver removes bilirubin from the blood and excretes it through bile. There are also many pediatric liver diseases including biliary atresia, alpha-1 antitrypsin deficiency, alagille syndrome, progressive familial intrahepatic cholestasis, and Langerhans cell histiocytosis, to name but a few. Diseases that interfere with liver function will lead to derangement of these processes. However, the liver has a great capacity to regenerate and has a large reserve capacity. In most cases, the liver only produces symptoms after extensive damage [8]. Liver diseases may be diagnosed by liver function tests, for example, by production of acute phase proteins shown in [Fig. 3].

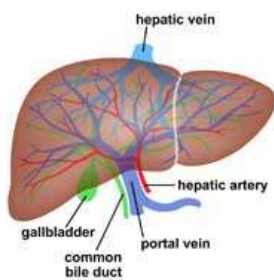


Fig. 3: Diagram of liver



Fig.4: Retina with exudates formation

marked by the masses of white or yellowish layer in the posterior part of the fundus oculi, with deposit of cholestrin and blood debris from retinal hemorrhage shown in [Fig. 4].

Exudates Detection

Exudates are appeared as bright yellow-white deposits on the retina due to the leakage of blood from abnormal vessels. Their shape and size will vary with different diseases according to the stages. The gray scale image is first preprocessed uniformly before the morphological image processing is applied to remove the blood vessels and identify the exudates region. The exudates are detected after removing the border, optical disk and non-exudates area shown in [Fig. 5].

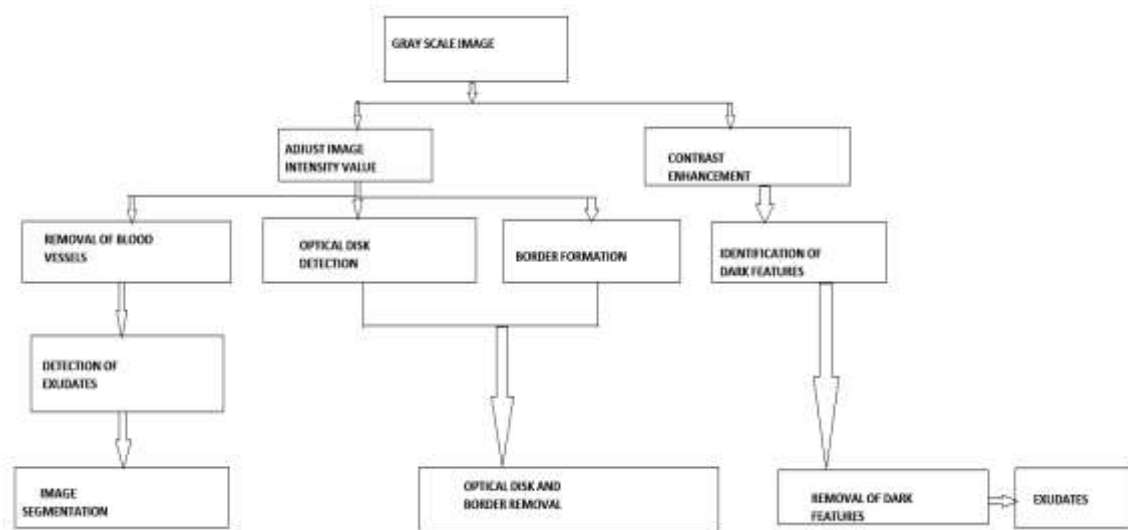


Fig.5: Exudates detection

First the fundus images is first preprocessed to standardize its size 576x720 and the intensity of the gray scale image is then adjusted. Morphological closing which consisted of dilate followed by erode is applied to remove blood vessels. The dilate function expands the exudates area while the erode function removes the blood vessels. The location of the optic disk is detected by the brightest point(s) on the gray scale image. It is usually the maximum value and a circular mask is then created to cover it. The regions of exudates are obtained after the removal of the circular border. Morphological closing is then applied to the image. The dilate function is to fill the exudates while erode function is to expand their sizes. Non-exudates (dark features) are extracted from the gray scale image using function and are represented as binary 1 (white) after intensity inversion. AND logic is then applied in the images to detect the exudates.

Experimental Procedure -AND LOGIC

AND logic is used to remove noise for the detection of exudates. Region with exudates are marked out after applying column filter but this includes non-exudates such as hemorrhage and has to be removed as noise. Then removing the non-exudates from the detected regions, the exudates can spots for comparison. These areas (bright features) are represented by binary 0 and the non-exudates (dark features) are represented by binary 1 (white) shown in [Fig. 6] and the corresponding values are shown in [Table 1].

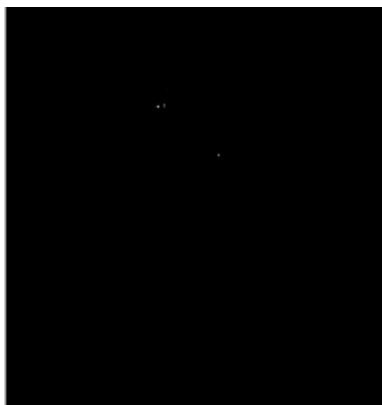


Fig. 6: Exudates

**Table 1:** Threshold Values For Exudates

AREA	ENERGY	CONTRAST	CORRELATION	HOMOGENITY	OUTPUT
258	0.269534	0.941772733	0.121151789	0.673930325	1
195	0.270413	0.936932381	0.123631085	0.671076344	1
193	0.300596	0.932133324	0.115210345	0.660918304	1
440	0.290851	0.933853832	0.127305377	0.673249401	1
447	0.290253	0.959611786	0.091914368	0.667889627	1
127	0.304575	0.951999322	0.099191053	0.663451239	1
409	0.31617	0.936177946	0.108731471	0.658349425	1
604	0.327915	0.949234444	0.09618857	0.656938872	1
181	0.287229	0.936293525	0.116746738	0.665477467	1
659	0.31674	0.942673083	0.096499257	0.655838107	1
344	0.357489	0.937330111	0.097130299	0.646802964	1
99	0.306969	0.952835069	0.095444083	0.663511605	0
272	0.323525	0.932548543	0.106329258	0.652542795	1
6	0.326471	0.936648733	0.108990078	0.657893424	0
64	0.274644	0.918994111	0.138176376	0.686375694	0
110	0.382856	0.935785889	0.092238385	0.635736322	1
48	0.351474	0.935184807	0.099805383	0.644807925	0

### Microaneurysm Detection

The gray scale image is first preprocessed uniformly before the morphological image processing is applied to remove the blood vessels and exudates and identify the microaneurysm region. The microaneurysms are detected after removing the border, optical disk and exudates area shown in [Fig. 7].



**Fig. 7:** Microaneurysm in retina

### Experimental Procedure:

First the fundus images are first preprocessed to standardize its size 576x720 and the intensity of the gray scale image is then adjusted. Morphological closing which consisted of dilate followed by erode is applied to remove blood vessels and microaneurysm. The dilate function expands the microaneurysm area while the erode function removes the blood vessels and microaneurysm. The location of the optic disk is detected by the brightest point(s) on the gray scale image. It is usually the maximum value and a circular mask is then created to cover it. The regions of microaneurysm are obtained after the removal of the circular border. Morphological closing is then applied to the image. The dilate function is to fill the microaneurysm while erode function is to expand their sizes. Exudates (dark features) are extracted from the gray scale image using function "im2bw" and are represented as binary 1 (white) after intensity inversion. AND logic is then applied in the images to detect the microaneurysm shown in [Fig. 8].

### Experimental Procedure -AND LOGIC:

AND logic is used to remove noise for the detection of microaneurysm. Region with microaneurysm are marked out after applying column filter but this includes exudates such as hemorrhage and has to be removed as noise. Then removing the exudates from the detected regions, the exudates can spots for comparison. These areas (bright features) are represented by binary 0 and the non-exudates (dark features) are represented by binary 1 (white) shown in [Fig. 9] and the corresponding values are shown in [Table 2].

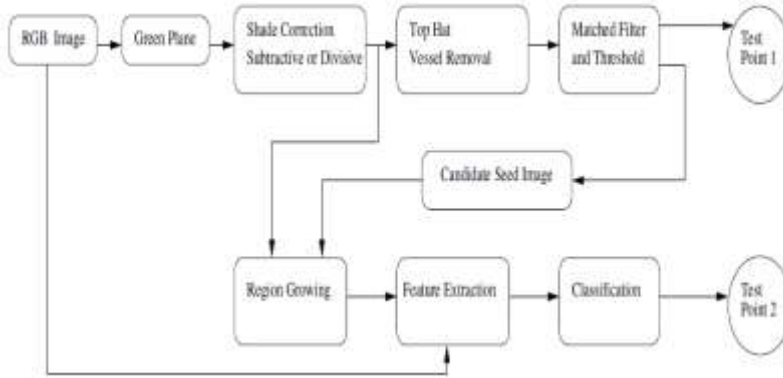


Fig. 8: block diagram for microaneurysm extraction

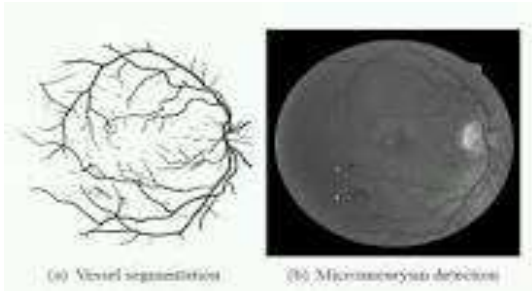


Fig. 9: vessel segmentation and microaneurysm structure.

Table 2: Threshold Values For Microaneurysm

AREA	ENERGY	CONTRAST	CORRELATION	HOMOGENITY	OUTPUT
344	0.357489	0.937320111	0.097130299	0.846802964	1
99	0.306869	0.952835068	0.095444089	0.863511605	0
272	0.323525	0.932546541	0.106329258	0.852542795	1
6	0.328471	0.936048735	0.108590078	0.857839424	0
64	0.274644	0.918994111	0.138176176	0.868375684	0
110	0.383856	0.935765669	0.092236365	0.835736322	1
48	0.351474	0.935184807	0.099605383	0.844807925	0
0	0.273335	0.927134808	0.1276279	0.879611996	0
276	0.362864	0.944921501	0.091267655	0.842319656	1
162	0.265922	0.932088982	0.125012536	0.872845918	1
33	0.274166	0.916474163	0.147005483	0.868018733	0
47	0.279434	0.936004474	0.128673513	0.867605913	0
8	0.340012	0.949237017	0.090816972	0.861026881	0
0	0.348957	0.926848875	0.108737955	0.846607098	0
8	0.323709	0.938626726	0.101828821	0.835786675	0
8	0.329555	0.944470804	0.100862242	0.85348679	0

### Training Adaptive Neuro-fuzzy inference system using the ANFIS editor GUI

The acronym ANFIS derives its name from *adaptive neuro-fuzzy inference system*. Using a given input/output data set, the toolbox function `anfisc` constructs a fuzzy inference system (FIS) whose membership function parameters are tuned (adjusted) using either a back propagation algorithm alone or in combination with a least squares type of method. This adjustment allows your fuzzy systems to learn from the data they are modeling shown in [Fig. 10].

The input retinal image is taken and selected for green plane. Retinal vessels are extracted by contrast limited adaptive histogram equalization and morphology and disease is thus observed. This helps clinicians to determine clearly about the type of diseases and thus provide the necessary treatment shown in [Fig. 11].

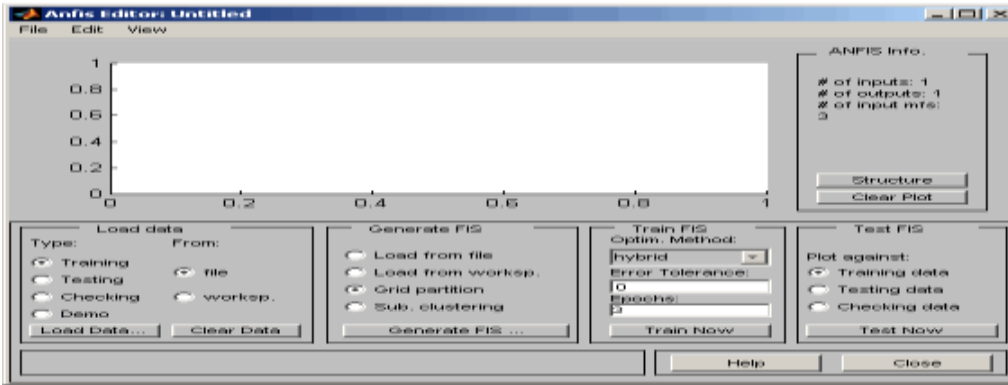


Fig.10: Training Adaptive neuro-fuzzy inference system output

## RESULTS

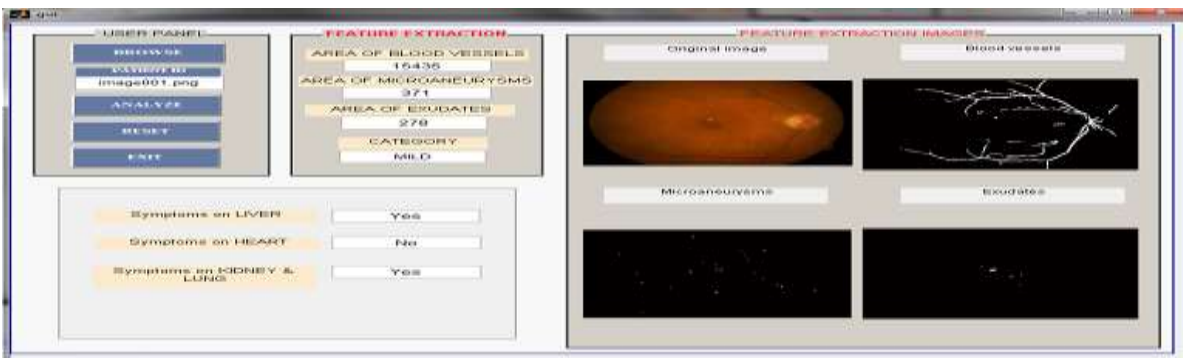


Fig.11: Simulation output

## CONCLUSION

Biomedical image processing requires an integrated knowledge in mathematics, statistics, programming and Biology. Different features of the fundus images namely Blood vessels, Exudates and Microaneurysms are extracted using image processing techniques. The values obtained are essential as they represent the image and are necessary in order to classify the images accurately. Based on the result of the classifier, this project has a sensitivity of 80% and specificity of 20%. It is able to achieve a fairly accurate classification for mild and higher stages, but not for normal class resulting in a possible high false alarm. This might be improved by fine tuning the threshold values used on the images and more images could be used to improve the overall system. In this work, we learnt various techniques of image processing and were able to extract the features namely blood vessels, exudates and microaneurysms and texture properties like area, energy, contrast, correlation and homogeneity from the fundus images.

### CONFLICT OF INTEREST

There is no conflict of interest.

### ACKNOWLEDGEMENTS

None.

### FINANCIAL DISCLOSURE

None.

## REFERENCES

- [1] Vyborny CJ, Giger ML and Nishikawa RM. [2000] "Computer aided detection and diagnosis of breast cancer," *Radiologic Clinics Amer N.* 38(4):725-740. Jul. 1, 10.1016/S0033-8389(05)70197-4, 0033-8389.
- [2] AntoBennet M, Sankar Babu G, Natarajan S. September [2015]. "Reverse Room Techniques for Irreversible Data Hiding", *Journal of Chemical and Pharmaceutical Sciences.* 08(03): 469-475.
- [3] AntoBennet M, Sankaranarayanan S, Sankar Babu G. August [2015]. "Performance & Analysis of Effective Iris Recognition System Using Independent Component Analysis", *Journal of Chemical and Pharmaceutical Sciences.* 08(03): 571-576.
- [4] AntoBennet M, Suresh R, Mohamed Sulaiman S. August [2015] "Performance & analysis of automated removal of head movement artifacts in EEG using brain computer interface", *Journal of Chemical and Pharmaceutical Research.* 07(08): 291-299.
- [5] AntoBennet M. June [2015] "A Novel Effective Refined Histogram For Supervised Texture Classification",

*International Journal of Computer & Modern Technology*. 01(02):67-73.

- [6] AntoBennet M, Srinath R, Raisha Banu A. April [2015] "Development of Deblocking Architectures for block artifact reduction in videos", *International Journal of Applied Engineering Research*. 10(09):6985-6991.
- [7] AntoBennet M & JacobRaglend. [2012] "Performance Analysis Of Filtering Schedule Using Deblocking Filter

For The Reduction Of Block Artifacts From MPEQ Compressed Document Images", *Journal of Computer Science*. 9:1447-1454.

- [8] AntoBennet M & JacobRaglend. [2011] "Performance Analysis of Block Artifact Reduction Scheme Using Pseudo Random Noise Mask Filtering", *European Journal of Scientific Research*. 66(1):120-129.